ISSN 1674-1056
http://cpb.iphy.ac.cn
http://iopscience.iop.org/cpb
中国物理 B
Chinese Physics
中国物理 Chinese Physics B

State-to-state dynamics of F(^{2}P)+HO($^2\Pi$)→O(^{3}P)+HF($^1\Sigma^+$) reaction on 1^3A" potential energy surface

Juan Zhao(赵娟), Hui Wu(吴慧), Hai-Bo Sun(孙海波), Li-Fei Wang(王立飞)
Citation: Chin. Phys. B . 2018, 27(2): 023102. **doi:** 10.1088/1674-1056/27/2/023102

Journal homepage: http://cpb.iphy.ac.cn; http://iopscience.iop.org/cpb

What follows is a list of articles you may be interested in

State-to-state quantum dynamics of N(^{2}D)+HD (v=0, j=0) reaction

Yong Zhang(张勇)
Chin. Phys. B . 2016, 25(12): 123104. **doi:** 10.1088/1674-1056/25/12/123104

Differential cross sections of positron—hydrogen collisions

Rong-Mei Yu(于荣梅), Chun-Ying Pu(濮春英), Xiao-Yu Huang(黄晓玉), Fu-Rong Yin(殷复荣), Xu-Yan Liu(刘旭焱), Li-Guang Jiao(焦利光), Ya-Jun Zhou(周雅君)
Chin. Phys. B . 2016, 25(7): 073401. **doi:** 10.1088/1674-1056/25/7/073401

State-to-state quantum dynamics of the N(^{4}S)+H_2 ($X^1\Sigma^+$)→NH($X^3\Sigma^-$)+H(^{2}S) reaction and its reaction mechanism analysis

Zhang Jing, Gao Shou-Bao, Wu Hui, Meng Qing-Tian
Chin. Phys. B . 2015, 24(8): 083104. **doi:** 10.1088/1674-1056/24/8/083104

State-to-state quantum dynamics of the N(^{4}S)+H_2 ($X^1\Sigma^+$)→NH($X^3\Sigma^-$)+H(^{2}S) reaction and its reaction mechanism analysis

Zhang Jing, Gao Shou-Bao, Wu Hui, Meng Qing-Tian
Chin. Phys. B . 2015, 24(8): 083104. **doi:** 10.1088/1674-1056/24/8/083104

Theoretical simulation of the photoassociation process for NaCs

Zhang Chang-Zhe, Zheng Bin, Wang Jun, Meng Qing-Tian
Chin. Phys. B . 2013, 22(2): 023401. **doi:** 10.1088/1674-1056/22/2/023401

State-to-state dynamics of $F(^2P) + HO(^2\Pi) \rightarrow O(^3P) + HF(^1\Sigma^+)$ reaction on $1^3A''$ potential energy surface*

Juan Zhao(赵娟)[1,2,†], Hui Wu(吴慧)[3], Hai-Bo Sun(孙海波)[1], and Li-Fei Wang(王立飞)[1]

[1] College of Science, Shandong Jiaotong University, Jinan 250357, China
[2] State Key Laboratory of Molecular Reaction Dynamics, Dalian Institute of Chemical Physics, Chinese Academy of Sciences, Dalian 116023, China
[3] College of Science, Jiangnan University, Wuxi 214122, China

(Received 29 September 2017; revised manuscript received 20 November 2017; published online 5 January 2018)

State-to-state time-dependent quantum dynamics calculations are carried out to study $F(^2P) + HO(^2\Pi) \rightarrow O(^3P) + HF(^1\Sigma^+)$ reaction on $1^3A''$ ground potential energy surface (PES). The vibrationally resolved reaction probabilities and the total integral cross section agree well with the previous results. Due to the heavy–light–heavy (HLH) system and the large exoergicity, the obvious vibrational inversion is found in a state-resolved integral cross section. The total differential cross section is found to be forward–backward scattering biased with strong oscillations at energy lower than a threshold of 0.10 eV, which is the indication of the indirect complex-forming mechanism. When the collision energy increases to greater than 0.10 eV, the angular distribution of the product becomes a strong forward scattering, and almost all the products are distributed at $\theta_t = 0^\circ$. This forward-peaked distribution can be attributed to the larger J partial waves and the property of the F atom itself, which make this reaction a direct abstraction process. The state-resolved differential cross sections are basically forward-backward symmetric for $v' = 0$, 1, and 2 at a collision energy of 0.07 eV; for a collision energy of 0.30 eV, it changes from backward/sideward scattering to forward peaked as v' increasing from 0 to 3. These results indicate that the contribution of differential cross sections with more highly vibrational excited states to the total differential cross sections is principal, which further verifies the vibrational inversion in the products.

Keywords: state-to-state quantum dynamics, time-dependent wave packet, differential cross section, $F(^2P) + HO(^2\Pi)$

PACS: 31.15.xv, 34.50.–s, 03.67.Lx **DOI:** 10.1088/1674-1056/27/2/023102

1. Introduction

As always, the reactions of atomic oxygen with hydrogen halides (HX, where H and X refer to hydrogen and halogen respectively) have received considerable attention for their importance in the studies of molecular reaction dynamics.[1–5] By disentangling the relative contributions in high-resolution angular and velocity distribution measurements at different collision energies, the dynamic behaviors of both $O(^3P)$ and $O(^1D)$ reactions have been investigated,[6] and the effect of electronic excitation on the reaction dynamics of atomic oxygen and the possible role of inter-system crossing between triplet and singlet potential energy surfaces have also been explored directly.

On account of the relatively simple electronic structure, the HOF system has often been chosen as a model system for open shell reactions and has been studied widely. Many important researches have been done by Gómez-Carrasco *et al.*,[7–31] including building the potential energy surface (PES), calculating the dynamics, and studying the photoionization. In 2004, Gómez–Carrasco *et al.* performed high-level MRCI electronic structure calculations for 8069 energy points to calibrate the fitted PES of the ground adiabatic $1^3A''$ triplet electronic state.[7] In the same year, they used the aug-cc-pVTZ extended basis sets given by Dunning *et al.* for the *ab initio* calculations obtaining a more accurate PES of the triplet $1^3A''$ electronic state.[8] According to this high-quality PES, they studied the dynamics of the $F(^2P) + HO(^2\Pi) \rightarrow O(^3P) + HF(^1\Sigma^+)$ reaction by quasi-classical trajectory (QCT) and wave packet methods,[7–9] and calculated the quantum state-to-state reaction probabilities[10] of the same reaction by using a newly proposed coordinate transformation method. In 2005, Gómez-Carrasco *et al.*[12] further reported the new PESs for the excited $2^3A''$ and $1^3A'$ triplet states and extended their previous dynamics study of the $F(^2P) + HO(^2\Pi) \rightarrow O(^3P) + HF(^1\Sigma^+)$ reaction by implementing wave packet calculations within the centrifugal sudden (CS) approximation on the excited triplet states. In 2006, the Gómez-Carrasco group developed the coupled diabatic potential energy surfaces[13] of $1^3A''$, $2^3A''$, and $1^3A'$, and calculated the angular resolved photodetachment cross sections of OHF. According to these diabatic potential energy surfaces, they compared the adiabatic dynamics with nonadiabatic dynamics of $F(^2P) + HO(^2\Pi) \rightarrow O(^3P) + HF(^1\Sigma^+)$ reactive collision,[14] and analyzed the final state distribution of

*Project supported by the National Natural Science Foundation of China (Grant Nos. 11504206 and 11404049), the China Postdoctoral Science Foundation (CPSF) (Grant No. 2014M561259), and the Ph. D. Research Start-up Fund of Shandong Jiaotong University.

†Corresponding author. E-mail: zhjuan2002@126.com

© 2018 Chinese Physical Society and IOP Publishing Ltd

products, obtaining that the OHF system can provide the opportunity to perform a nonadiabatic study with the coupled electronic states involved. Later, in 2007, they constructed the first five adiabatic singlet states ($2^1A'$, $3^1A'$, $1^1A''$, $1^1A'$, and $2^1A''$) of the OHF system,[15] and studied the photoelectron detachment process of OHF at 213 nm. The ground adiabatic $1^1A'$ singlet PES is further employed in the subsequent quasi-classical trajectory and the wave packet calculation of $O(^1D)+HF \rightarrow OH+F(^2P)$.[16]

Using the above PESs of the HOF system, many researches about the dynamics of this system have been done. Gogats[17] performed three-dimensional (3D) real wave packet calculations for the $H(^2S)+FO(^2\Pi) \rightarrow OH(^2\Pi)+F(^2P)$ reaction based on the $1^3A''$ and $1^3A'$ state PESs, and obtained the integral cross sections, the initial state selected reaction probabilities and reaction rate constants for total angular momentum $J=0$. Recently, our group has studied the relative reactions occurring on $1^3A''$ PES of the OHF system by using the QCT method. We analyzed the product rotational polarization and the isotope effect of the stereo-dynamics, etc., of H + FO, F + HO, and O + HF reactions[18–21] and obtained some valuable information about chemical reaction stereo-dynamics. In addition, Chu *et al.* have studied the vector properties of the $O(^1D)+HF \rightarrow OH+F(^2P)$ reaction on the PES of the $1^1A'$ singlet state and the stereodynamics of reactions $H/D+FO \rightarrow OH/OD+F$, $HF/DF+O$ using three PESs of the $1^1A'$, $1^3A'$, and $1^3A''$ states by the time-dependent quantum wave packet and QCT method;[22,23] while Zhao *et al.* have investigated the stereodynamic behaviours of H + OF and F + HO reactions on the above three PESs by using the QCT method,[24,25] analyzing the influence of collision energy, isotopic effects and initial excitation effects on the $H+OF \rightarrow HO+F$ reaction.[26]

The above studies about the HOF system mainly focus on the state-to-all dynamics of related reactions. However, when two molecules collide, the state-to-state quantum reaction dynamic study can reveal a more detailed observable and profound insight into the chemical reaction process. So, it is very necessary to calculate the state-to-state quantum for the considered reaction system. As far as we know, there have been few studies into state-to-state dynamic behaviors of the title reaction except in Ref. [10], where Gómez-Carrasco *et al.* calculated only the quantum state-to-state reaction probabilities for the title reaction for total angular momenta $J=0$ and 60 by using a time-dependent method in a body-fixed frame; they found that the total energy was nearly equally distributed between translation and vibration of products, with very little excitation of rotations, and obtained the rovibrationally resolved state-to-state reaction probabilities for $J=0$ and 60. In order to analyze in more detail the dynamics, we here investigate the product state-resolved integral cross sections (ICSs) and differential cross sections (DCSs) of $F(^2P)+HO(^2\Pi) \rightarrow O(^3P)+HF(^1\Sigma^+)$ on the $1^3A''$ PES with all Js considered. The rest of this paper is organized as follows. In Section 2, we give the theoretical method to be used in this work. In Section 3 we present the results and discussion, and finally we draw some conclusions from the present study in Section 4.

2. Theoretical method

Recently, the programs for the state-to-state quantum scattering dynamics were developed by Zhang and Han.[27–29] In the present paper, the efficient GPUs version of the TDWP[27] code is used. The Hamiltonian of the title reaction is defined in the body-fixed (BF) product Jacobi coordinates. For a given J (J is the total rotational angular momentum), the Hamiltonian can be expressed as ($\hbar=1$)

$$\hat{H}=-\frac{\hbar^2}{2\mu_R}\frac{\partial^2}{\partial R^2}-\frac{\hbar^2}{2\mu_r}\frac{\partial^2}{\partial r^2}+\frac{\left(\hat{J}-\hat{j}\right)^2}{2\mu_R R^2}+\frac{\hat{j}^2}{2\mu_r r^2}+V_{\rm pes}, \quad (1)$$

where R is the distance between O and the center of mass of HF; r is the bond length of HF; μ_r is the corresponding reduced mass and is expressed as $\mu_r=m_F\cdot m_H/(m_F+m_H)$; μ_R can be written as $\mu_R=m_O\cdot(m_H+m_F)/(m_O+m_H+m_F)$; $\hat{J}$ is the total angular momentum operator; $\hat{j}$ is the rotational angular momentum operator of HF; $V_{\rm pes}$ is the potential energy of the FHO system.

The initial Gaussian wave packet for the reactant in the space-fixed (SF) reactant Jacobi coordinate is expanded as

$$|\chi_i\rangle=\varphi^{JM\varepsilon}_{\alpha v_0 j_0 l_0}=G(R_\alpha)\,\phi_{v_0 j_0}(r_\alpha)\,|JMj_0l_0\varepsilon\rangle\,. \quad (2)$$

For the initial state $(v_0j_0l_0)$, $|JMj_0l_0\varepsilon\rangle$ represents the SF rotational basis and describes the angular motion, with M being the projection of the total angular momentum J. The $\phi_{v_0j_0}(r_\alpha)$ is the rovibrational eigenfunction of the diatomic molecule HO. With the initial wavepacket, the propagation of this wavepacket is entirely calculated on the graphics processing units (GPUs) in BF product Jacobi coordinates with rotational function $|JMj_0K\rangle$, with K being the projection of total angular momentum J in BF coordinates, and the initial wavepacket at the grid $\left(R_{v0},r_{vi},\theta_{vj},K_\beta\right)$ in the BF product Jacobi coordinate is

$$\begin{aligned}&\Psi(R_{v_0},r_{v_i},\theta_{v_j},K_\beta)\\&=\sum_{K_\alpha}\Psi\left(R_\alpha(R_{v_0},r_{v_j},\theta_{v_j}),r_\alpha(R_{v_0},r_{v_j},\theta_{v_j}),\theta_\alpha(R_{v_0},r_{v_j},\theta_{v_j})\right)\\&\quad\times d^{J\varepsilon^*}_{K_\beta K_\alpha}.\end{aligned}$$

Then, this wave function begins to propagate in the BF product Jacobi coordinates in the split-operator scheme

$$\begin{aligned}&\Psi^{JMp}(\boldsymbol{R},\boldsymbol{r},t+\Delta)\\&=\exp\left(-\mathrm{i}\hat{H}_0\frac{\Delta}{2}\right)\exp\left(-\mathrm{i}\hat{V}_{\rm rot}\frac{\Delta}{2}\right)\exp(-\mathrm{i}V\Delta)\\&\quad\times\exp\left(-\mathrm{i}\hat{V}_{\rm rot}\frac{\Delta}{2}\right)\exp\left(-\mathrm{i}\hat{H}_0\frac{\Delta}{2}\right)\varphi^{JMp}(\boldsymbol{R},\boldsymbol{r},t), \quad (3)\end{aligned}$$

$$\hat{H}_0 = -\frac{\hbar^2}{2\mu_R}\frac{\partial^2}{\partial R^2} - \frac{\hbar^2}{2\mu_r}\frac{\partial^2}{\partial r^2} + V_r(r), \quad (4)$$

$$\hat{V}_{\rm rot} = \frac{(\hat{J}-\hat{j})^2}{2\mu_R R^2} + \frac{\hat{j}^2}{2\mu_r r^2}, \quad (5)$$

where $V_r(r)$ is the potential energy of HF.

The radial component of the product wavepacket is a delta function multiplied by the outgoing asymptotic radial function

$$|\chi_{\rm f}\rangle = \delta(R-R_\infty)\phi_{v_{\rm f}j_{\rm f}}(r_\beta)\,|JMj_{\rm f}l_{\rm f}\rangle\,, \quad (6)$$

where R_∞ is the fixed radial coordinate in the asymptotic region. So, the scattering matrix element in BF representation is defined as

$$S_{\rm fi}(E) = \frac{1}{2\pi a_{\alpha\,\rm i}(E)a^*_{\beta\,\rm f}(E)}\int {\rm d}t\,{\rm e}^{({\rm i}/\hbar)Et}\,\langle\chi_{\beta\,\rm f}|\,{\rm e}^{({\rm i}/\hbar)\hat{H}t}\,|\chi_{\alpha\,\rm i}\rangle. \quad (7)$$

The coefficients are given by

$$a_{\alpha\,\rm i}(E) = \langle\phi_{\rm i}|\chi^+_{\rm i}\rangle = \left\langle {\rm i}\sqrt{\frac{\mu_R k_{\alpha\,\rm i}}{2\pi}}R{\rm h}^{(2)}_{l_\alpha}(k_{\alpha\,\rm i}R)|G(R_\alpha)\right\rangle, \quad (8)$$

$$a_{\beta\,\rm f}(E) = \langle\phi_{\rm f}|\chi^+_{\rm f}\rangle = \left\langle \sqrt{\frac{\mu_R k_{\beta\,\rm f}}{2\pi}}R{\rm h}^{(1)}_{l_\beta}(k_{\beta\,\rm f}R)|\delta(R-R_\infty)\right\rangle, \quad (9)$$

where $\rm h^{(1,2)}$ are the spherical Hankel functions of the first and second kinds. Finally, the scattering matrix is transformed into helicity representation to derive the DCS and ICS by a scattering matrix summing over all relevant total angular momentum quantum number J.

$$\frac{{\rm d}\sigma_{v'j',v_0j_0}(\theta,E)}{{\rm d}\Omega} = \frac{1}{(2j_0+1)}\sum_{K'}\sum_{K_0}\left|\frac{1}{2{\rm i}k_{v_0j_0}}\sum_J(2J+1)d^J_{K'K_0}(\theta)S^J_{v'j'K',v_0j_0K_0}\right|^2, \quad (10)$$

$$\sigma_{v'j',v_0j_0} = \frac{1}{(2j_0+1)k^2_{v_0j_0}}\sum_{K'}\sum_{K_0}\sum_J(2J+1)\times\left|S_{v'j'K',v_0j_0K_0}\right|^2, \quad (11)$$

where $k_{v_0j_0}$ is the translational wave vector of the initial state (v_0, j_0), θ is the scattering angle, and $d^J_{K'K_0}$ is the Wigner rotational matrix.

Using this method, the quantum state-to-state dynamics of many reactions has been successfully studied and a large amount of valuable information has been obtained.[30–33]

In the present work, we carry out the state-to-state calculations for all angular momentum Js values up to 140 to converge differential cross sections of the title reaction for collision energies up to 0.80 eV. To insure convergence of scattering results, extensive tests have been carried out to determine the optimal parameters, which are summarized in Table 1. One of the key convergence parameters in this work is denoted as K. This parameter sets an upper limit to the helicity quantum number. Table 2 shows the convergence tests on the K for selected J and higher collision energy $E_{\rm C} = 0.60$ eV. It can be seen that the number of K ($K = \min(10, J+1)$) is sufficiently large to yield converged results.

Table 1. Numerical parameters used in the present quantum wave packet calculations.

Parameter	Value
Product Jacobi coordinate (R) range	2.0–18.0 a_0
No. grid points in R	300
No. translational basis functions in the interaction region	200
Product Jacobi coordinate (r) range	1.0–22.0 a_0
No. grid points in r	185
No. vibrational basis functions in the interaction region	120
No. angular grid points	150
Center of initial wave packet (R_0)	10.4 a_0
Width of the wave packet (δ)	0.161 a_0
Integration time interval (Δ)	2.5 a.u.
Absorption length in R and r	4.0/4.0 a_0
Absorption strength in R and r	0.03/0.03
Position for flux analysis in R and r	13.5/10.0 a_0
Propagation time	60000 a.u.

Table 2. Convergence test of F + HO($v_0 = 0$, $j_0 = 0$) → HF(v', j') + O reaction probabilities as a function of K (with $E_{\rm C} = 0.60$ eV and $J = 30$, 60, and 90).

$E_{\rm C} = 0.60$ eV	K	Total	HF(v', all j') + O				
			$v'=0$	$v'=1$	$v'=2$	$v'=3$	$v'=4$
$J=30$	8	0.13358265	0.03373300	0.03180328	0.02150117	0.04274873	0.00379647
	10	0.13358314	0.03373302	0.03180950	0.02150252	0.04273178	0.00380632
	12	0.13354529	0.03373643	0.03181859	0.02149644	0.04271616	0.00377767
$J=60$	8	0.17707975	0.02894937	0.02912954	0.04789848	0.07047739	0.00062497
	10	0.17708394	0.02909003	0.02903478	0.04795410	0.07039593	0.00060911
	12	0.17708721	0.02909356	0.02906808	0.04790722	0.07041381	0.00060455
$J=90$	8	0.12526367	0.00397327	0.01807556	0.05276344	0.05011492	0.00033649
	10	0.12547303	0.00447903	0.01880616	0.05204223	0.04978330	0.00036231
	12	0.12561086	0.00453590	0.01888586	0.05199310	0.04982578	0.00037023

3. Results and discussion

3.1. Reaction probability and reaction cross section

The $F(^2P)+HO(^2\Pi) \rightarrow O(^3P)+HF(^1\Sigma^+)$ reaction is very exoergic, and the detailed information about the existence of PES of $1^3A''$ ground electronic state can be seen in Ref. [8]. The main characteristic is a low barrier at a bent geometry and two wells: one is in the entrance channel with a bent geometry and the other is in the product channel with a linear geometry, which makes the reaction present two different mechanisms: one is direct at energy above the transition state zero point energy, i.e., at about 0.10 eV, and the other is below this threshold indirectly mediated by HLH resonances.[8,10,11] These resonances are associated with the periodic orbits at the transition state.[8]

Firstly, in order to verify our calculation correctness, the vibrationally resolved reaction probabilities are calculated for $J=0$ and $J=60$, which are shown in Fig. 1. Our results are in good agreement with the ones calculated by Gómez-Carrasco *et al.* (see Ref. [10]). Thus, we can conclude that the calculation in this work is correct.

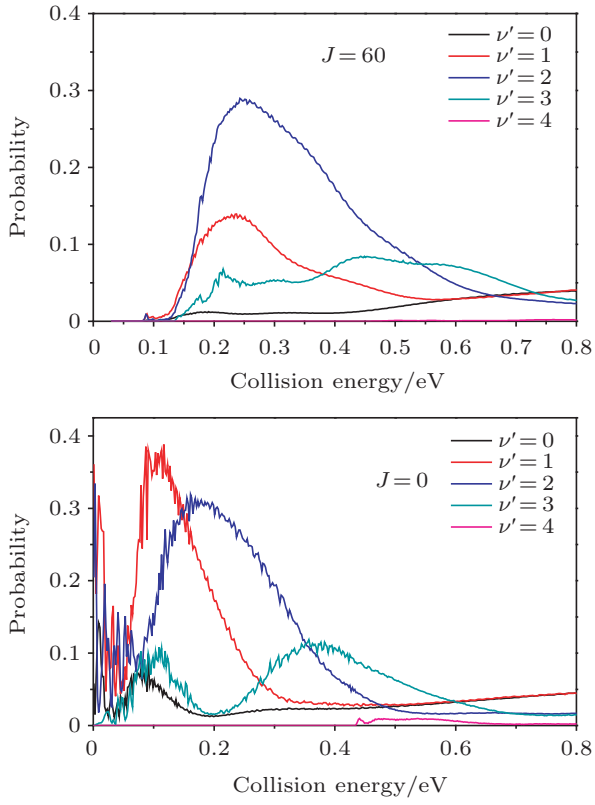


Fig. 1. (color online) Vibrationally state-resolved reaction probabilities for $F+HO(v=0,\ j=0) \rightarrow HF(v')+O$ collision at $J=0$ (lower panel) and $J=60$ (upper panel).

Figure 2 shows the total reaction probabilities for several partial waves. The resonance structure is very obvious for the smaller J, especially below the threshold at 0.10 eV; these resonances are typical in heavy-light-heavy systems and are associated with periodic orbits at the transition station.[8,10] As J increases, the distribution is shifted towards higher energies and the probability decreases, due to the increase of centrifugal barrier with J increasing. Then resonances gradually wear off and nearly disappear at higher J (60 and more).

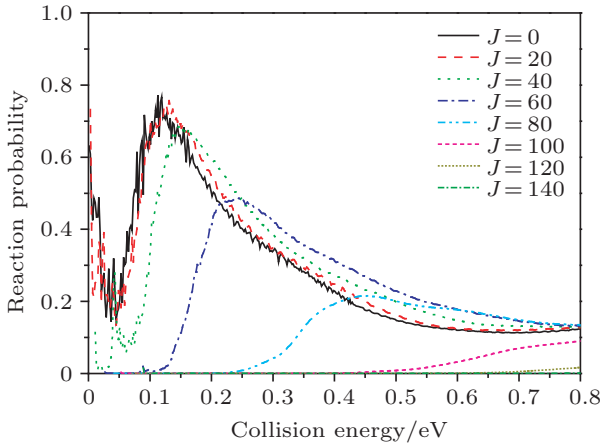


Fig. 2. (color online) Variations of total QM reaction probability with collision energy for the $F+HO \rightarrow HF+O$ reaction at several J values.

In order to determine whether those resonances persist in the reaction cross section, the total reaction cross section for $F+HO(v=0,j=0)$, in Fig. 3, is calculated by adding all partial waves through using the time-dependent wave packet (TDWP) quantum method including the split-operator scheme. The red solid line represents the TDWP results in this work, and the other results are cited from Ref. [8]. From this figure it follows that all the total reaction cross section presents two parts, (one is at energies above the transition state zero point energy, at about 0.10 eV, and the other is below this threshold), which are associated with the direct and indirect mechanisms, respectively. The comparison between the TDWP and CSA [8] results shows their qualitative behaviors are in agreement well with each other. Below the threshold about 0.10 eV, the indirect mechanism dominates, and the reaction cross section

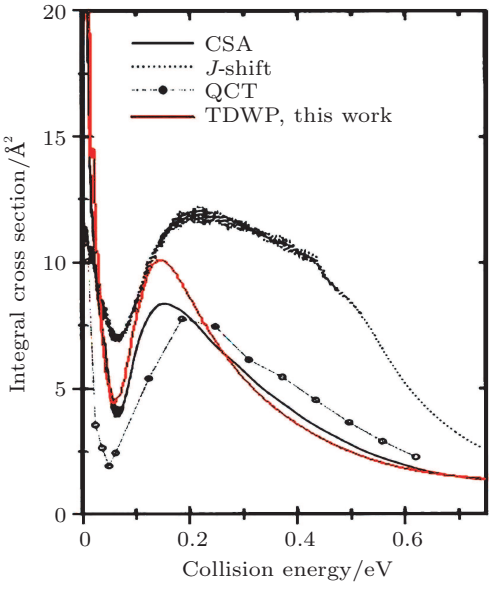


Fig. 3. (color online) Variations of total reaction cross section versus collision energy for the $F+HO(v=0,j=0)$ collision. The red line represents our results, the CSA, J-shifting, and QCT results are cited from Ref. [8].

is very large. Above this threshold energy, the reaction cross section grows rapidly to a maximum value at about 0.15 eV for both methods. Beyond this maximum the reaction cross section decreases nearly monotonically as expected for exoergic reactions. In addition, there are some differences: above 0.10 eV, the TDWP results are slightly larger than the CSA ones and the peak obtained by the TDWP method is higher; at this point, the TDWP results agree well with the J-shift results, with collision energy further increasing. For the energies above 0.25 eV, the results from TDWP and CSA methods are in good agreement. The CSA and quantum wave packet ("exact") methods were also used to calculate the reaction probability for $J = 40$ by Gómez-Carrasco *et al.*[8] The CSA method, in which a single helicity quantum number is considered, indeed underestimates the probability, while in our TDWP calculation, the maximum value of the helicity quantum number reaches 10.

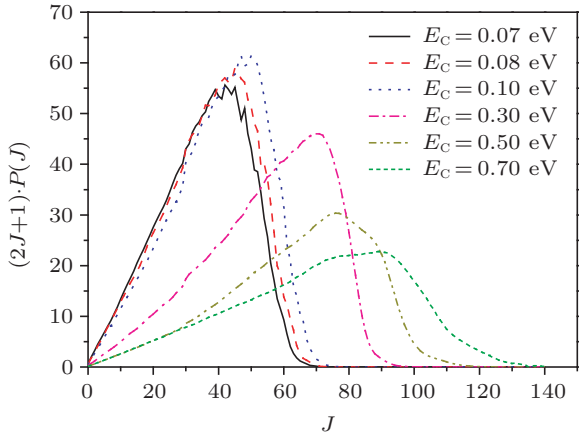


Fig. 4. (color online) $(2J+1)$ weighted opacity functions for F + HO → FH + O reaction at different collision energies.

To shed light on the J dependence of the total reaction probabilities, we plot the reaction probabilities at six collision energies versus the total angular momentum in Fig. 4. The J-dependent partial wave contribution is weighted over a $(2J+1)$ factor to the integral cross section. It is well known that the J dependence of the integral cross sections is analogous to the opacity function $p(b)$. Thus, different J dependence means different impact parameter dependence. In the low energy region, ($E_C \leq 0.1$ eV), where the indirect mechanism is dominated, the $(2J+1)P$ value rapidly increases and reaches a maximum value near $J = 50$, and then sharply decreases to zero before J reaches the last accessible value. Moreover, there are several resonances in these three cases, and the peak becomes higher and higher with the collision energy increasing. A similar tendency also exists in the high energy region, ($E_C > 0.1$ eV), i.e., $(2J+1)P$ value first increases and then decreases, but the peak becomes lower with the increase of collision energy, which is expected for the exergonic reaction, the reaction probability decreases as collision energy increases.

3.2. Product distribution

The calculated product HF vibrational distributions for the title reaction in a collision energy range from 0.07 eV to 0.80 eV are shown in Fig. 5, which are obtained by summing all available rotational state populations in each vibrational channel. For the cases of $v' < 4$, the obvious vibrational inversion is observed in Fig. 5. The main maxima in the v' distribution ($v' = 1$, 2, and 3 for 0.1, 0.3, and 0.6, respectively) appear with increasing total energy. As reported in Ref. [10], because of the HLH system and the large exoergicity, the energy of this reaction is nearly equally distributed between translation and vibration of products, with very little excitation of rotations. In addition, the direct mechanism dominates at the saddle point and the system presents the approximately orthogonal modes in their ground state, which induces the vibrational excitation and inversion.

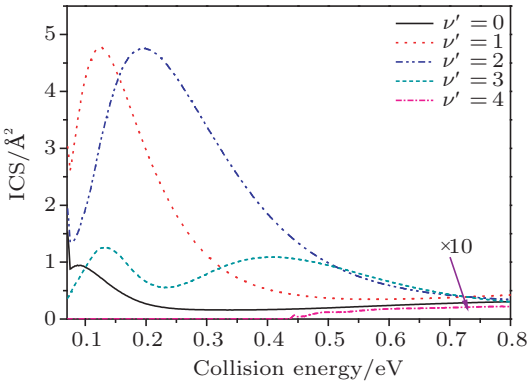


Fig. 5. (color online) Vibrational state-resolved reaction cross sections for the F + HO($v = 0$, $j = 0$) → HF(v') + O collision. Curve has been multiplied by a factor of 10 for the case of $v' = 4$.

The rotational state-resolved reaction cross sections of the HF product are also calculated and shown in Fig. 6. There is a similar tendency for all collision energies, i.e., each reaction cross section becomes smaller and smaller with j' increasing. Comparing Fig. 5 with Fig. 6, the vibrationally resolved state-to-state reaction cross sections have high-order magnitudes, which further confirms the above conclusion (much more translation energy is converted into the vibrational energy).

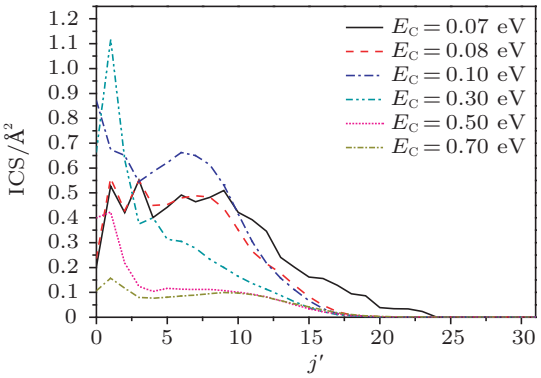


Fig. 6. (color online) Rotational state-resolved reaction cross sections for the F + HO($v = 0$, $j = 0$)→ HF(j') + O collision.

In order to provide much more indicative views of product vibrational and rotational state distributions, we plot 3D diagrams in Figs. 7 and 8. As can be seen in Fig. 7, the products mainly concentrate in a range between $v' = 1$ and 2 and $j' < 15$, which is in good accordance with the distributions in Figs. 5 and 6. Figure 8 shows the vib-rotational distribution at each energy more clearly: below 0.10 eV, there are mainly three vibrational levels ($v' = 1$, 2, and 3), while above this energy, the product is mainly distributed at one vibrational level (at $v' = 2$, 3, and 3 for 0.30, 0.50, and 0.70 eV, respectively). For collision energy lower than 0.10 eV, the indirect mechanism dominates and there will be a complex form, thus there is not enough energy to stimulate the product to too high an excited state. While for collision energy higher than 0.10 eV, the direct mechanism dominates, which promotes the vibrational excitation. It can also be seen in Fig. 8 that the rotational distribution has no inversion, so there are more products at the lower rotational energy-level.

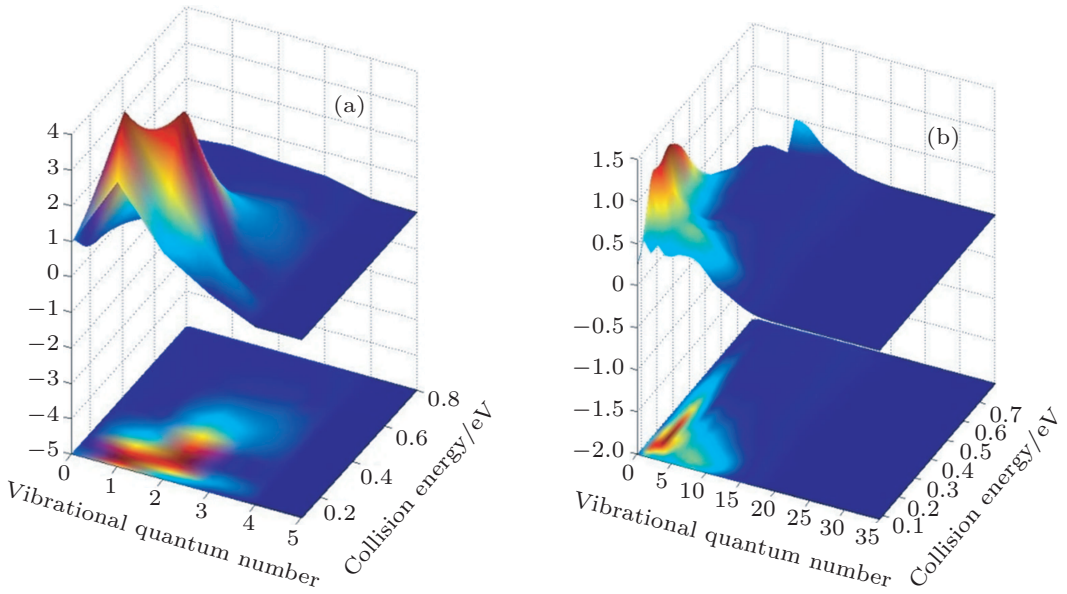


Fig. 7. (color online) 3D product vibrational state-resolved reaction cross section (left panel), and 3D product rotational state-resolved reaction cross section (right panel).

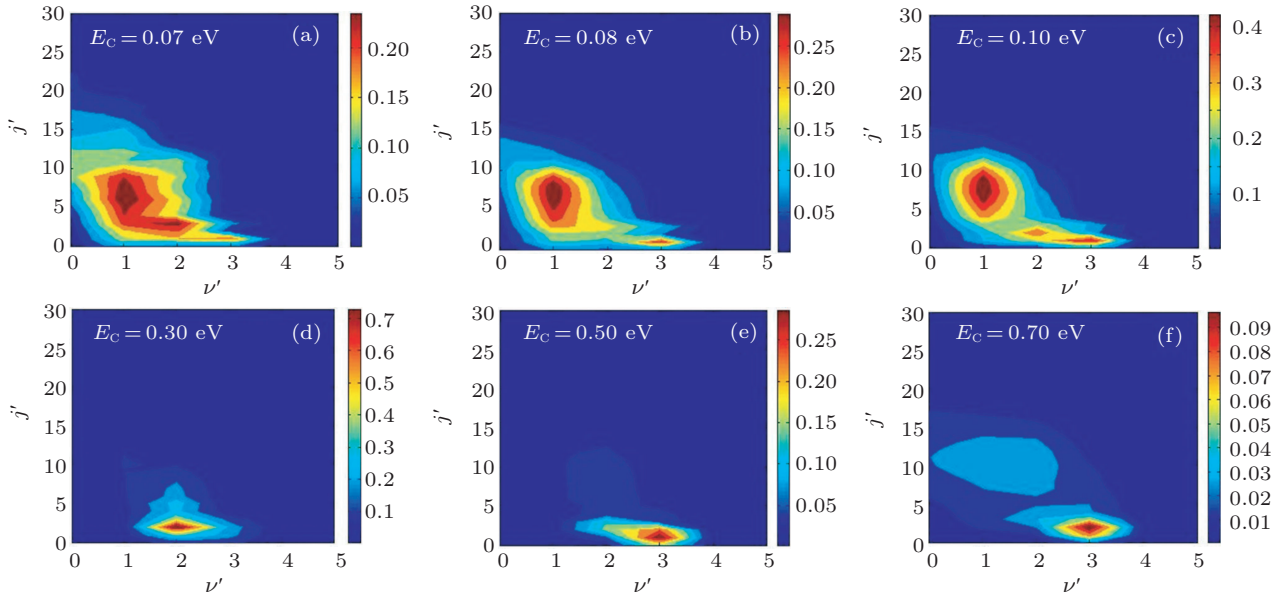


Fig. 8. (color online) Product ro-vibrational state-resolved distributions at several collision energies.

3.3. Differential cross sections

Figure 9 displays the calculated total DCSs of the F + HO($v = 0, j = 0$) reaction in two energy regions: one is $E_C \leq 0.1$ eV (0.07, 0.08, and 0.10 eV), called the low energy region; the other is $E_C > 0.1$ eV (0.30, 0.50, and 0.70 eV), called the high energy region. It is apparent that the angular distribution favors the forward scattering for the high collision energy, while it gives an almost forward-backward symmetric pattern for the low collision energy. The symmetric pattern is probably due to the dominant complex formation mechanism

that allows the molecules to rotate in the [OHF] well in different directions. Meanwhile, when collision energy becomes slightly large, the side scattering begins to exist and the backward scattering becomes stronger; this is because the rebound mechanism begins to play a major role. In addition, several oscillations can be seen which may be attributed to the indirect mechanism mediated by HLH resonance. As the collision energy further increases, in the high energy region, a larger number of partial waves are involved in the reaction as shown in Fig. 4, which suggests that the contribution from the direct abstraction mechanism becomes larger. Alternatively, in the classical scattering item, the maximum impact parameter (b_{max}) has a one-to-one relationship with the total angular momentum J. Further, according to the "osculating complex" model,[34–36] the collisions at the large impact parameter lead to "semi-trapped" complex with short lifetime. Considering our reaction system, the F atom is much heavier than the H atom, and it has a relatively strong absorbability to charge. The F atom will rapidly and easily grip the H atom away from the HO molecule, and directly produce HF molecule, which induces the very strongly forward scattering.

Finally, in order to further explore the details, the state-resolved DCSs at two corresponding typical collision energies are given in Fig. 10, which reveals more angular structures than the total reactive DCSs. In this figure, it can be seen that the product state-specific DCSs are obviously dependent on collision energy. For the low-energy case, $E_C = 0.07$ eV (note the break on vertical axis), the angular distributions for $v' = 0$, 1, and 2 states are dominated by forward and backward scattering and the much stronger forward scattering can be seen in the $v' = 3$ case, that is, all the vibrational excited HF ($v' = 1$, 2, and 3) and ground HF ($v' = 0$) states contribute to the forward scattering component, but HF with $v' = 3$ is little help to backward scattering. Moreover, with v' increasing, the maximum value of j' becomes smaller and smaller, which is related to the preference for forming the vibrational excited products in the title reaction. For the energy above the threshold, $E_C = 0.30$ eV (note the difference in color scale among these four plots), the product distribution is mainly backward scattering and sideways scattering for $v' = 0$ and 1, respectively, but these tendencies are very weak, when v' increases, the forward scattering becomes more and more obvious, until it reaches forward peaked scattering at the $v' = 3$ state, that is, the forward peaked scattering of the total DCS for 0.30 eV in Fig. 9 is due to the high vibrational excited ($v' = 3$) products. Although the integral cross sections at $v' = 1$ and 2 are much larger (see Fig. 5), the tendencies of backward scattering and sideways scattering are both too weak to present backward scattering or sideways scattering tendency in the total DCS. In this case, the direct abstraction mechanism is predominant, and more translational energy is converted into the vibrational energy. Moreover, the decrease of the maxima of j' with v' increasing is also found in Fig. 10.

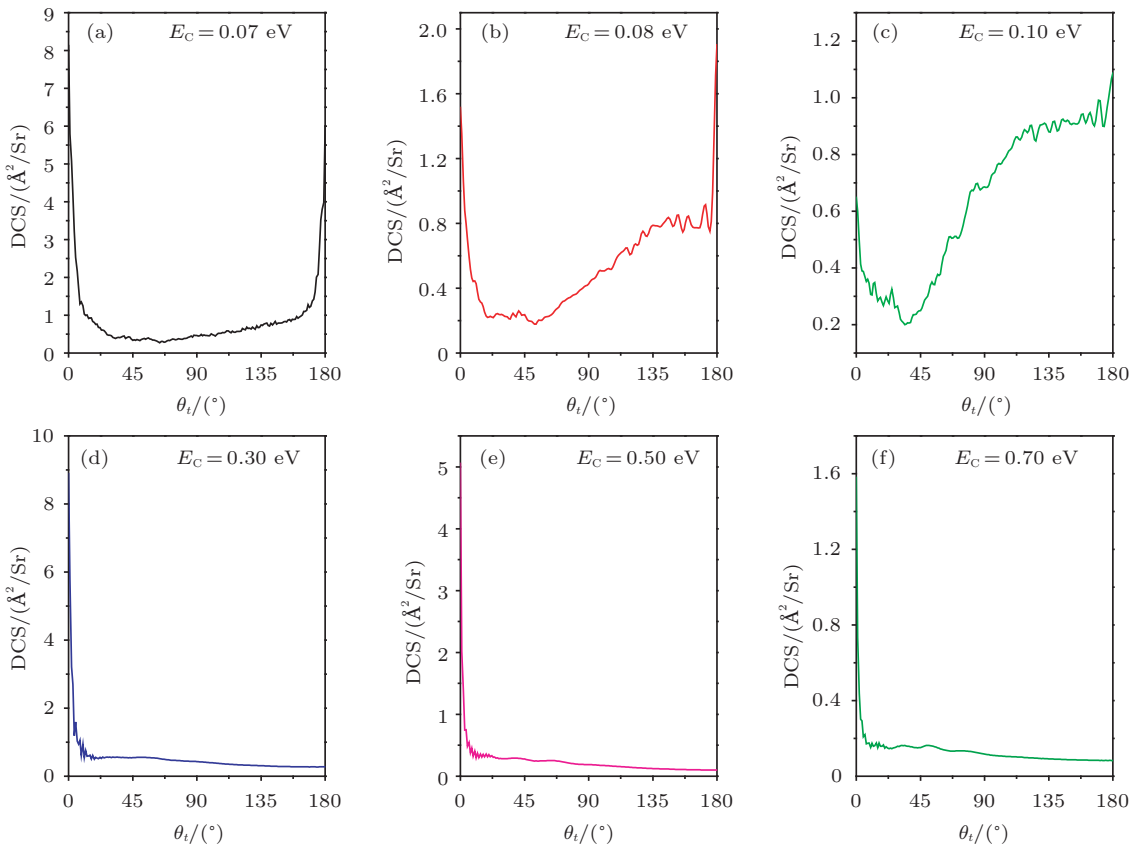


Fig. 9. (color online) Total DCSs for the F + HO → HF + O reaction at six collision energies.

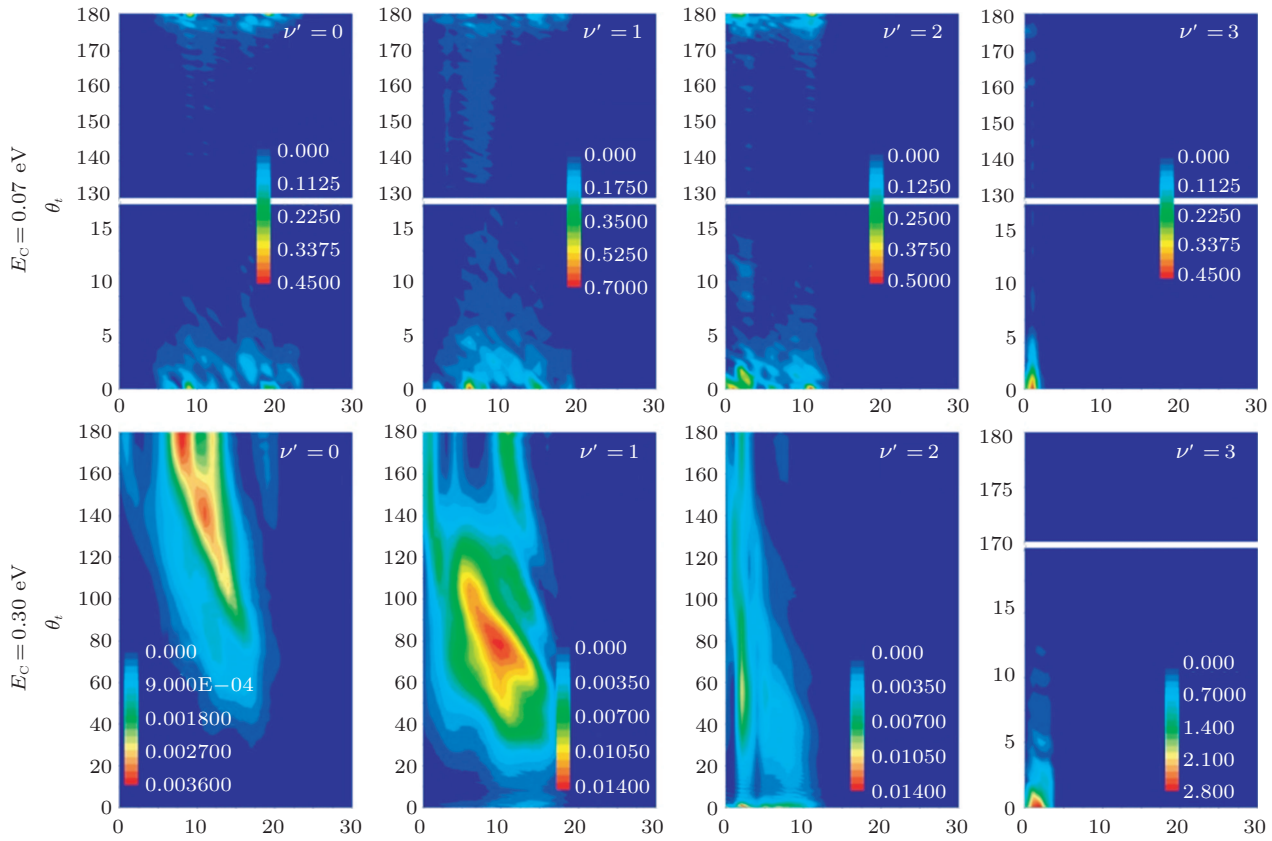


Fig. 10. (color online) State-resolved DCSs for the F + HO → HF + O reaction at two typical collision energies. Upper panels are for collision energy of 0.07 eV; lower panels for collision energy of 0.30 eV.

4. Conclusions

In this work, an efficient GPU version of time-dependent wave-packet code is used to calculate the differential cross section of $F(^2P) + HO(^2\Pi) \rightarrow O(^3P) + HF(^1\Sigma^+)$ reaction on the ground state $1^3A''$ PES. The vibrationally resolved reaction probabilities of $J = 0$ and $J = 60$ and the integral cross section are in good agreement with earlier results.[8,10] Obvious resonances are found in reaction probability for smaller J, especially in the low collision energy region, which are associated with the indirect mechanism mediated by HLH resonances. The quantum state-resolved reaction probability and cross section calculations demonstrate that the product vibrational state distributions are typically inverted, differing from the non-inverted rotational distributions. This is mainly because of the HLH mass combination. The larger rotational constant corresponds to the diatomic molecule, formed by a light H atom and a much heavier atom such as O or F, and most of the rotational energy is carried by OH or HF. Therefore, before and after reaction, $L \approx L'$, and their rotational constants are relatively very low.[10] Finally, total and state-resolved DCSs are also calculated. At low collision energies, the HF products are predominantly forward/backward scattered due to the low impact parameter b collision and indirect complex forming mechanism. At high collision energies, the direct abstraction mechanism is more inclined to produce forward scattering and furnish a high vibrational excitation of the HF.

References

[1] Balucani N, Beneventi L, Casavecchia P and Volpi G G 1991 *Chem. Phys. Lett.* **180** 34
[2] Han K L and He G Z 2007 *J. Photochem. Photobio. C: Photochem. Rev.* **8** 55
[3] Tsurumaki H, Fujimura Y and Kajimoto O 2000 *J. Chem. Phys.* **112** 8338
[4] Balucani N, Casavecchia P, Stranges D and Volpi G G 1993 *Chem. Phys. Lett.* **211** 469
[5] Alagia M, Aquilanti V, Ascenzi D, Balucani N, Cappelletti D, Cartechini L, Casavecchia P, Pirani F, Sanchini G and Volpi G G 1997 *Isr. J. Chem.* **37**329
[6] Girard Y and Chaquin P 2003 *J. Phys. Chem. A* **107** 10462
[7] Gómez Carrasco S, González Sánchez L and Aguado A 2004 *Chem. Phys. Lett.* **383** 25
[8] Gómez Carrasco S, González Sánchez L and Aguado A 2004 *J. Chem. Phys.* **121** 4605
[9] González Sánchez L, Gómez Carrasco S, Aguado A, Paniagua M, Luz Hernánder M, Alariño J M and Roncero O 2004 *Mol. Phys.* **102** 2381
[10] Gómez Carrasco S and Roncero O 2006 *J. Chem. Phys.* **125** 054102
[11] Gómez Carrasco S, Roncero O and González Sánchez L 2004 *J. Chem. Phys.* **121** 309
[12] González Sánchez L, Gómez Carrasco S and Aguado A 2005 *J. Chem. Phys.* **123** 114310
[13] Gómez Carrasco S, Aguado A, Paniagua M and Roncero O 2006 *J. Chem. Phys.* **125** 164321
[14] Zanchet A, González Lezana T, Aguado A, Gómez Carrasco S and Roncero O 2010 *J. Phys. Chem.A* **114** 9733
[15] Gómez Carrasco S, Aguado A, Paniagua M and Roncero O 2007 *J. Photochem. Photobiol. A* **190** 145
[16] Gómez Carrasco S, Hernández M L and Alvarinõ J M 2007 *Chem. Phys. Lett.* **435** 188

[17] Gogtas F 2008 *J. Comput. Chem.* **29** 1889
[18] Zhao J, Xu Y, Yue D G and Meng Q T 2009 *Chem. Phys. Lett.* **471** 160
[19] Meng Q T, Zhao J, Xu Y and Yue D G 2009 *Chem. Phys.* **362** 65
[20] Zhao J, Xu Y, Yue D G and Meng Q T 2009 *J. Phys. B: At. Mol. Opt. Phys.* **42** 165006
[21] Zhao J, Xu Y and Meng Q T 2010 *Acta Phys. Sin.* **59** 144 (in Chinese)
[22] Chu T S, Zhang H, Yuan S P, Fu A P, Si H Z, Tian F H and Duan Y B 2009 *J. Phys. Chem. A* **113** 3470
[23] Chu T S 2010 *J. Comp. Chem.* **31** 1385
[24] Zhao D, Zhang T Y and Chu T S 2010 *Can. J. Chem.* **88** 893
[25] Zhao D, Chu T S and Hao C 2012 *J. Mole. Mode.* **18** 3283
[26] Zhao D, Chu T S and Hao C 2013 *Chin. Phys. B* **22** 063401
[27] Zhang P Y and Han K L 2013 *J. Phys. Chem. A* **117** 8512
[28] Zhang P Y and Han K L 2014 *J. Phys. Chem. A* **118** 8929
[29] Zhang P Y and Han K L 2015 *Int. J. Quantum Chem.* **115** 738
[30] Wu H, Yao C X, He X H and Zhang P Y 2016 *J. Chem. Phys.* **144** 184301
[31] Wu H, Duan Z X, Yin S H and Zhao G J 2016 *J. Chem. Phys.* **145** 124305
[32] Zhang J, Gao S B, Wu H and Meng Q T 2015 *J. Phys. Chem. A* **119** 8959
[33] Zhang Y 2016 *Chin. Phys. B* **25** 123104
[34] Song H W, Lee S Y, Sun Z G and Lu Y P 2013 *J. Chem. Phys.* **138** 054305/1
[35] Shen Z T, Cao J W and Bian W S 2015 *J. Chem. Phys.* **142** 164309
[36] Xie W, Liu L, Sun Z, Guo H and Dawes R 2015 *J. Chem. Phys.* **142** 064308